Spin transport in a graphene normal-superconductor junction in the quantum Hall regime

Tibor Sekera,[1] Christoph Bruder,[1] and Rakesh P. Tiwari[2]

[1]*Department of Physics, University of Basel, Klingelbergstrasse 82, CH-4056 Basel, Switzerland**

[2]*Department of Physics, McGill University, 3600 rue University, Montreal, Quebec, Canada H3A 2T8*

(Dated: October 11, 2018)

The quantum Hall regime of graphene has many unusual properties. In particular, the presence of a Zeeman field opens up a region of energy within the zeroth Landau level, where the spin-up and spin-down states localized at a single edge propagate in opposite directions. We show that when these edge states are coupled to an s-wave superconductor, the transport of charge carriers is spin-filtered. This spin-filtering effect can be traced back to the interplay of specular Andreev reflections and Andreev retro-reflections in the presence of a Zeeman field.

PACS numbers: 81.05.ue, 73.43.-f, 73.20.At, 74.45.+c

I. INTRODUCTION

Monolayer graphene has remarkable electronic transport properties. One of them is a peculiar quantum Hall effect, which can be observed even at room temperature[1]. Inducing superconductivity via the proximity effect further enriches these transport properties[2–4]. Recently, a number of experiments have performed conductance measurements in the quantum Hall regime in monolayer graphene, using superconducting electrodes[5–7]. Moreover, coupling the helical edge states within the zeroth Landau level in graphene to an s-wave superconductor can also give rise to Majorana bound states[8,9].

Low-energy excitations in graphene reside in two disconnected regions in the first Brillouin zone, known as valleys. In the quantum Hall regime, the energy spectrum has an unconventional Landau level (LL) structure, where the LL energies are proportional to $\pm\sqrt{n}$ with integer n. This discrete set of flat Landau levels develop into dispersive edge states towards the edge of a sample. In the low-energy approximation, the bulk LL energies in graphene are given by

$$E_n^\xi = \lambda\hbar\omega_c\sqrt{n}\,, \tag{1}$$

where the valley index $\xi = \pm$ denotes the $K^\pm$ valley, and $\lambda = \pm 1$ labels the conduction and valence band, respectively. The cyclotron frequency is given by $\hbar\omega_c = \sqrt{2}\hbar v_F/\ell_B$, where v_F is the Fermi velocity, $\ell_B = \sqrt{\hbar/(eB)}$ is the magnetic length and $B = |\mathbf{B}|$ is the absolute value of the applied magnetic field; n is a non-negative integer. These bulk LLs are four-fold degenerate: two-fold for the spin and two-fold for the valley degree of freedom. The valley degeneracy is lifted at the edge of the sample, where the boundary condition for the wavefunction couples the valleys[10–14]. Hence the zeroth Landau level (ZLL) splits into two spin-degenerate bands, one with positive and one with negative energies, see Figs. 1(a) and (b).

If the spin degeneracy is lifted by, e.g., a Zeeman field, each of the LLs splits into two with energy difference $2\Delta_Z$, where $\Delta_Z = \frac{1}{2}g^*\mu_B B$. Here, g^* is the effective g-factor of an electron in graphene and μ_B is the Bohr magneton. The energy difference between the spin-up and spin-down bulk LLs is $2\Delta_Z \approx 2.3\,\mathrm{meV}$ at $B \sim 10\,\mathrm{T}$ for the interaction-enhanced g-factor, $g^* = 4$, see Refs. 12,15. Close to the edge, the spin splitting leads to spin-up and spin-down edge states propagating in opposite directions in the energy region $-\Delta_Z < E < \Delta_Z$, see Figs. 1(c) and (d). Such a system can be used as a spin filter. In Ref. 12, the authors propose a four-terminal device where the spin-filtering effect can be achieved by inducing backscattering between the counter-propagating edge states locally (using gates) in just one part of the system. The spin-filtering effect takes place due to the presence of an in-plane magnetic field and spin-orbit coupling.

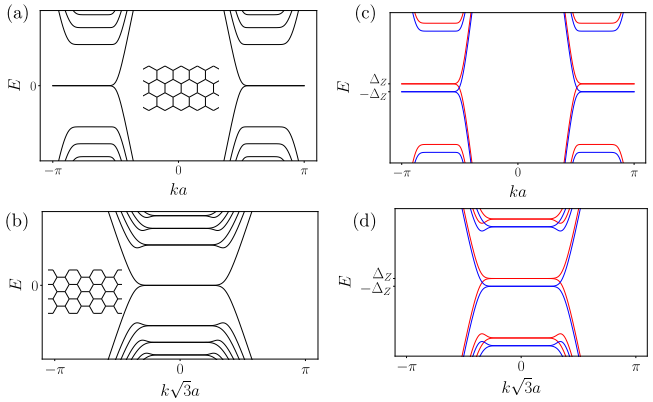

FIG. 1: Electron band structures of the few lowest Landau levels[12]. (a) Band structure of a zigzag ribbon, (b) of an armchair ribbon. The ribbons are shown in the insets. (c) and (d) The corresponding band structures in the presence of a Zeeman field that splits the energies for spin-up (red) and spin-down (blue) electrons.

Here, we suggest a different mechanism for the spin-filtering effect. We couple the edge states to an s-wave superconductor with a critical field high enough such that superconductivity and the quantum Hall effect coexist, and consider only subgap transport. The Andreev-reflected hole can have the same or the opposite direction

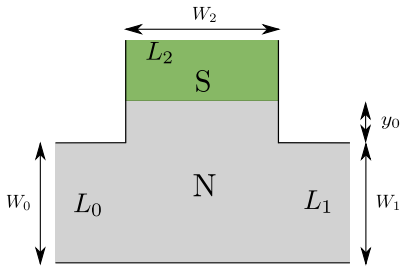

FIG. 2: A graphene ribbon in the normal state (gray region N) with two leads L_0 and L_1 and a superconducting lead L_2 (green region S) attached to the top edge. The width of the lead L_i is denoted by W_i. An external magnetic field smaller than the critical field of the superconductor is applied such that the normal region is in the quantum Hall regime. The superconductor couples electron and hole edge states propagating along the upper edge. We assume that a bias voltage V is applied between leads L_0 and L_1.

of propagation as the electron impinging on the interface with the superconductor at energy E. Which case is realized depends on the nature of the Andreev reflection in graphene that can be a retro-reflection for $E < E_F$ or a specular reflection for $E > E_F$, see Ref. 16. Hence, if an incoming spin-down electron is specularly reflected while the spin-up electron is retro-reflected, spin-filtering takes place. We demonstrate this effect in the three-terminal device shown in Fig. 2. This is done by employing a tight-binding model on a honeycomb lattice within the Bogoliubov-De Gennes (BdG) framework and taking into account the orbital and spin effect of the magnetic field. Note that the present work is related to but different from the idea in Ref. 17. There, the charge component of a spin-polarized current is filtered away by using specular Andreev processes in the absence of an external magnetic field. However, the authors need a ferromagnetic lead to initially generate the spin-polarized current.

The rest of this article is organized as follows. In Sec. II we describe the setup of a three-terminal device and introduce its Hamiltonian. The transport coefficients of this structure are introduced and determined in Sec. III. We discuss and summarize our results in Sec. IV and conclude in Sec. V.

II. MODEL

We investigate spin transport in the three-terminal device shown in Fig. 2. The underlying honeycomb lattice with lattice constant a is exposed to a quantizing out-of-plane magnetic field. The upper edge of the system is coupled to an s-wave superconductor (S) with a sizeable critical field, such that the quantum Hall effect and superconductivity coexist[5–7]. There are two normal leads L_0 and L_1 of widths W_0 and W_1, respectively, which serve to probe the spin-resolved transmission through the scattering region. In the rest of the paper, $W_0 = W_1 = W$. The superconducting lead L_2 effectively creates a normal-superconducting interface of length W_2 that converts electrons to holes. The geometry of the system is motivated by a recent experiment[6].

The tight-binding Hamiltonian of the system can be written as

$$H = H_0 + H_\Delta + H_Z \,, \tag{2}$$

where

$$\begin{aligned} H_0 =& \sum_{\langle ij\rangle} \psi_i^\dagger \Big[-te^{i\varphi_{ij}} \frac{1}{2}(\eta_0 + \eta_z) \\ &+ te^{-i\varphi_{ij}} \frac{1}{2}(\eta_0 - \eta_z) \Big] \otimes s_0 \psi_j \\ &- E_F \sum_i \psi_i^\dagger (\eta_z \otimes s_0) \psi_i \,, \\ H_\Delta =& \sum_i \Delta_i \psi_i^\dagger (\eta_x \otimes s_0) \psi_i \,, \\ H_Z =& \sum_i \Delta_{Zi} \psi_i^\dagger (\eta_0 \otimes s_z) \psi_i \,. \end{aligned} \tag{3}$$

The four-spinor field ψ_i is in the standard Nambu basis $\psi_i = (c_{i\uparrow}, c_{i\downarrow}, c_{i\downarrow}^\dagger, -c_{i\uparrow}^\dagger)^T$, where $\psi_i^\dagger$ creates a particle localized at site i with a four-component wavefunction $(\chi_{e\uparrow}(\mathbf{r}-\mathbf{r}_i), \chi_{e\downarrow}(\mathbf{r}-\mathbf{r}_i), \chi_{h\uparrow}(\mathbf{r}-\mathbf{r}_i), -\chi_{h\downarrow}(\mathbf{r}-\mathbf{r}_i))^T$. Here, the index es (hs) denotes an electron (hole) with spin $s \in \{\uparrow, \downarrow\}$. The two sets of Pauli matrices, η_ν and s_ν with $\nu \in \{0, x, y, z\}$, describe the electron-hole and spin degree of freedom, respectively. Finally, $\sum_i$ and $\sum_{\langle ij\rangle}$ denote sums over all sites and over nearest neighbors.

The first (second) term in H_0 describes the nearest-neighbor hopping of electrons (holes) in an out-of-plane magnetic field with a hopping amplitude $-te^{i\varphi_{ij}}$ ($te^{-i\varphi_{ij}}$). The Peierls phase is given by

$$\varphi_{ij} = -\frac{2\pi}{\phi_0} B \frac{y_i + y_j}{2} (x_j - x_i) \,, \tag{4}$$

where $\phi_0 = h/e$ is the magnetic flux quantum and (x_i, y_i) are the real-space coordinates of site i. The vector potential in the Landau gauge is chosen to be constant along the x-axis, $\mathbf{A} = (-By, 0, 0)$. The third term in H_0 represents the Fermi energy E_F of the system. In undoped graphene, $E_F = 0$.

The s-wave superconducting pairing is represented by H_Δ and couples an electron with spin s to a hole with spin s on the same lattice site. The Zeeman field described by H_Z splits each energy level into two with energy difference $2\Delta_Z$. For simplicity, we assume the spatial dependence of the pair potential Δ_i and of the magnetic field B_i to be a step function. That is, $\Delta_i = \Delta(y)$ ($B_i = B(y)$) is assumed to be a non-zero constant (zero) in the graphene sheet below the superconducting electrode and zero (a non-zero constant) otherwise. The magnitude of the Zeeman term has the same spatial dependence as the magnetic field.

In the following, we will calculate the scattering matrix for the system shown in Fig. 2. All the numerical results for the conductances and spin polarizations presented below were obtained using Kwant[18].

III. TRANSPORT COEFFICIENTS

In Figs. 3(a)–(c) we plot the relevant transport coefficients in the case when $E_F < \Delta_Z < \Delta$ and the gap between the ZLL and other LLs is large enough so that only the ZLL plays a role. Since the Hamiltonian in Eq. (2) conserves the z-projection of the spin, $[H, s_z] = 0$, only the spin-diagonal transport coefficients are shown. The transmission coefficient for a particle with spin up scattered to a particle with spin up is shown in red, while blue is used for spin-down particles. T_{ee} (T_{he}) is the probability for an electron from L_0 to be scattered into an electron (a hole) in L_1 and R_{he} is the probability for an electron from L_0 to be backscattered as a hole to L_0. Because we are in the quantum Hall regime and our system is wide enough, the probability for an electron from L_0 to be backscattered as an electron is zero ($R_{ee} = 0$) and hence not shown. It can be seen that for energies $|E| < \Delta$, the scattering matrix is unitary and $T_{ee} + T_{he} + R_{he} = 1$ for each spin projection.

It is interesting to look at the spin polarization of the carriers in the subgap regime, where $|E| < \Delta$. Since H conserves the spin projection along the z-axis, we define the spin polarization as

$$P = \frac{T_{e\uparrow,e\uparrow} + T_{h\uparrow,e\uparrow} - T_{e\downarrow,e\downarrow} - T_{h\downarrow,e\downarrow}}{T_{e\uparrow,e\uparrow} + T_{h\uparrow,e\uparrow} + T_{e\downarrow,e\downarrow} + T_{h\downarrow,e\downarrow}}\,, \tag{5}$$

where $T_{\alpha's',\alpha s}$ is the transmission coefficient for a particle α with spin s in lead L_0 to a particle α' with spin s' in lead L_1. To avoid numerical artifacts, we set $P = 0$ if the denominator in Eq. (5) is smaller than 10^{-3}, i.e., if almost no particle is transmitted from L_0 to L_1. The numerically calculated spin polarization is non-zero in the energy region $E_F - \Delta_Z < E < E_F + \Delta_Z$ and zero otherwise, see Fig. 3(e). This can be understood by looking at the bandstructure and the propagation direction of the particles along the edges of the sample as illustrated in Figs. 4(a) and (b), respectively. In the energy region II, a spin-up electron $e\uparrow$ travels undisturbed along the lower edge into L_1, however a spin-down electron $e\downarrow$ propagating along the upper edge is backscattered to L_0 as a spin-down hole $h\downarrow$ because a superconductor is coupled to the upper edge. This results in the accumulation of spin-up particles in L_1. The situation in the energy region I is the same for spin-down electrons $e\downarrow$. However, here a spin-up electron $e\uparrow$ also travels along the upper edge and encounters the superconductor. Since an Andreev-reflected spin-up hole $h\uparrow$ has the same propagation direction as a spin-up electron $e\uparrow$, the particle propagates along the GS interface via Andreev edge states, and, depending on the geometry, ends up with a certain probability as a spin-up electron $e\uparrow$ or spin-up

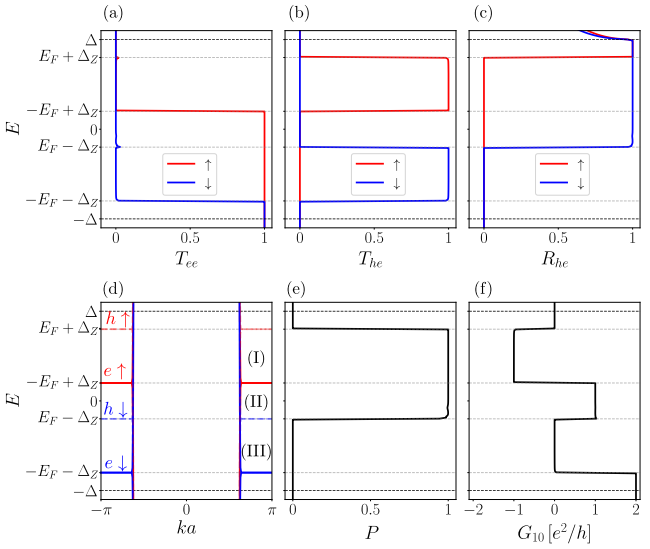

FIG. 3: On the horizontal axis, we plot in (a)–(c) the transport coefficients T_{ee}, T_{he}, and R_{he} for spin-up (red) and spin-down (blue) particles as a function of energy E (vertical axis). Similarly, (d) shows the band structure of the spin-split zeroth Landau level for electrons (full lines) and holes (dashed lines) of the normal lead L_0, (e) the spin polarization, both as a function of E. (f) (differential) charge conductance as a function of $E = eV$ where V is the bias voltage applied between leads L_0 and L_1. The thin horizontal dashed lines mark the energies where the edge states change the direction of propagation, while the thick ones correspond to $|E| = \Delta$. Here, the edge terminations of L_0 and L_1 are zigzag while the edge termination of L_2 is armchair. The parameters are $\Delta = 10\,\mathrm{meV}$, $E_F = 0.3\Delta$, $\Delta_Z = 0.5\Delta$, $B = 10\,\mathrm{T}$, $W = 600a$, $W_2 = 510a$, and $y_0 = 300a$.

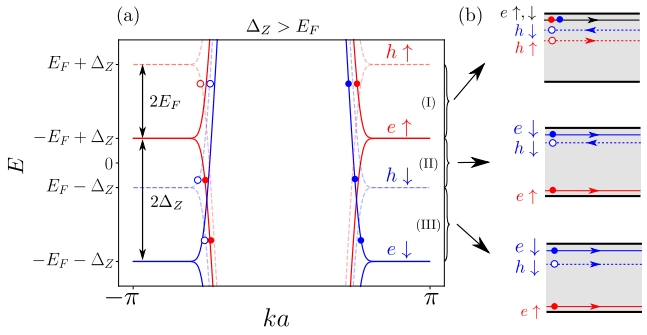

FIG. 4: (a) Band structure of electrons (full lines) and holes (dashed lines) of the spin-split zeroth Landau level for spin up (red) and spin down (blue) in a graphene zigzag ribbon. (b) Electron and hole edge states in lead L_0 and their propagation direction indicated by arrows shown for the three energy regions I–III. While there are four edge states at each edge, we show only the states relevant for the transport in our geometry (see Fig. 2). The representative electron (full circle) and hole state (empty circle) for spin up (red) and spin down (blue) in each energy region is shown in (a) as well as in (b).

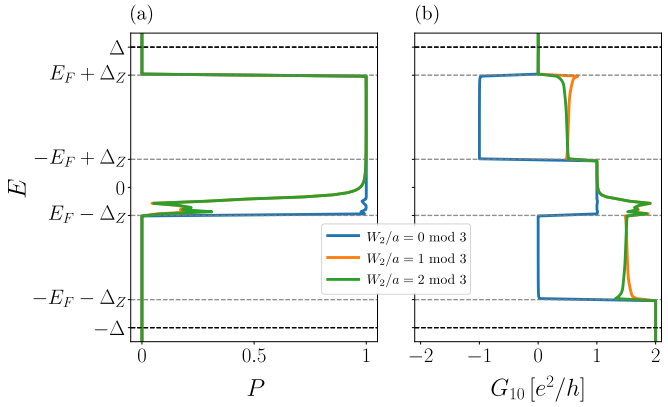

FIG. 5: (a) Spin polarization and (b) (differential) charge conductance for three different interface lengths (values of W_2) that correspond to three different valley polarizations. The charge conductance depends on the angle between the valley isospins, while the spin polarization does not (up to the region where $(e\downarrow)$ leaks to L_1 due to the smaller induced gap.) Here, $\Delta = 20\,\text{meV}$, $E_F = 0.3\Delta$, $\Delta_Z = 0.5\Delta$, $B = 10\,\text{T}$, $W = 600a$, and $y_0 = 300a$.

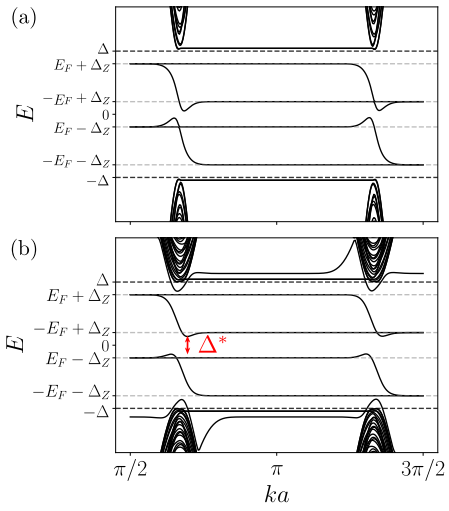

FIG. 6: (a)–(b) Band structure of excitations along the graphene-superconductor interface in a quantizing magnetic field for $\Delta/t = 0.05$ and 0.1, respectively. Dispersing states at the interface for $|E| < \Delta$ evolve into the flat zeroth Landau level (ZLL) away from the interface. The bulk ZLL is split into four: electrons and holes are coupled via the superconductor, while the spin degeneracy is lifted due to the Zeeman field. The interface states are valley-degenerate since the interface is smooth on the scale of the lattice constant. When $E_F < \Delta_Z$, the ZLL edge states develop an effective band gap Δ^* (red arrows) due to the coupling to a superconductor. Δ^* increases from (a) to (b) with increasing superconducting pair potential Δ. Here, $E_F = 0.3\Delta$, $\Delta_Z = 0.5\Delta$, and the interface is along the zigzag direction. The parameters Δ and magnetic field are chosen to be larger than their realistic values to obtain better visibility.

hole $h\uparrow$ in L_1. Thus, injecting spin-unpolarized particles in L_0 results in spin-polarized particles in L_1 in the energy region $E_F - \Delta_Z < E < E_F + \Delta_Z$.

We would now like to discuss the (differential) charge conductance. Here and in the following, we assume the temperature to be $T = 0$. Therefore, the energy E is experimentally given by the bias voltage, $E = eV$, where V is the potential difference between the leads L_0 and L_1. In the presence of hole excitations, the charge conductance from L_0 to L_1 is defined as

$$G_{10} = \frac{e^2}{h} \sum_{s=\uparrow,\downarrow} \left(T_{es,es} - T_{hs,es}\right) , \tag{6}$$

which is shown for our system in Fig. 3(f). In the energy region (I) the carrier ending in L_1 is a hole and $G_{10} = -e^2/h$, while in the region II it is an electron and $G_{10} = e^2/h$. In the energy region III there is a spin-up electron $e\uparrow$ along the lower edge and a spin-up hole $h\uparrow$ along the upper edge propagating into L_1, which results in zero charge transfer and $G_{10} = 0$. The charge conductance behavior, however, is not universal and depends on the valley structure of the edge states[13].

IV. DISCUSSION

In Fig. 5 we show the spin polarization and conductance for three different widths W_2 of lead L_2 which is assumed to have armchair edge termination. We see that the spin polarization is (almost) independent of the interface length W_2, while the charge conductance has a threefold character, depending upon the total number of hexagons across the width of the armchair ribbon being a multiple of three, or a multiple of three plus/minus one[13]. Besides that, a set of dips (peaks) in the spin polarization (conductance) for energies close to $E_F - \Delta_Z$ can be observed. This feature is due to a spin-down electron $e\downarrow$ leaking from L_0 to L_1 through the interface (without being Andreev-reflected). This can be understood as follows. Without the superconductor, there are edge states propagating in opposite directions for opposite spins. When we couple the superconductor to the upper edge, the electron impinging on the interface will be reflected as a hole (in the case of non-zero Andreev reflection probability). However, this hole propagates in the direction opposite to the electron edge state (for both spin projections) in this energy region. Hence, the transport along the interface should be blocked. But if the Andreev reflection probability is less than one, the electron has a finite chance to leak along the interface onto the other side. In other words, edge states along the upper edge contacted to a superconductor develop an effective gap[8] Δ^* that is smaller than the naively expected gap $2(\Delta_Z - E_F)$ (for $(\Delta_Z - E_F) < \Delta$). The bigger the pairing Δ, the higher the Andreev reflection probability. Thus, on increasing Δ, Δ^* approaches $2(\Delta_Z - E_F)$ as shown in Fig. 6.

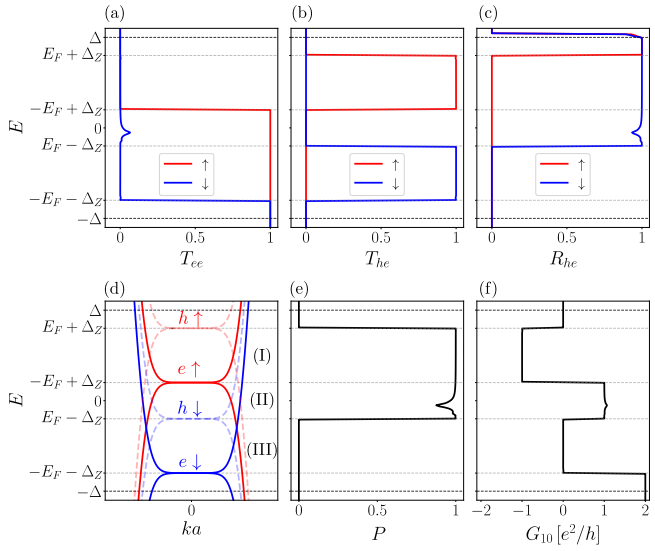

FIG. 7: Same as Fig. 3 but with armchair edge terminations for L_0 and L_1 and zigzag edge termination for L_2.

The spin-filtering effect for $|E| < \Delta$ is lost once the gate voltage shifts the Fermi energy such that it exceeds $\Delta + \Delta_Z$, i.e., the propagation direction of the electron and hole states is the same within the subgap region.

We obtain similar results if leads L_0 and L_1 have armchair orientation and lead L_2 has zigzag orientation, see Fig. 7. The spin polarization in Fig. 7(e) is again (nearly) perfect for $E_F - \Delta_Z < E < E_F + \Delta_Z$. This is expected since, unlike the valley structure, the spin structure of the ZLL in graphene is independent of the type of the edge termination. The conductance profile in Fig. 7(f) matches the one in Fig. 5(b) for $W_2/a = 0 \bmod 3$, which is the result of the same valley structure for the states at the edges of the NS interface for the two cases. The dip in the spin polarization is present for the same reason as in Fig. 5.

In the absence of the superconducting proximity effect ($\Delta = 0$ in the graphene sheet), the spin filtering takes place in the energy region $-E_F - \Delta_Z < E < -E_F + \Delta_Z$ and the hole excitations play no role. The spin-filtering effect is lost for $\Delta_Z = 0$, i.e., when the spin degeneracy is restored.

V. CONCLUSION

We have shown that spin filtering can be achieved by coupling the edge states of the spin-split zeroth Landau level in graphene to a superconductor. The spin-filtering effect can be switched on and off by applying a (global) gate voltage that shifts the Fermi energy. Unlike the charge conductance, the spin polarization is independent of the edge termination. The device can be put in different regimes by tuning the Zeeman energy independently of the gap between the zeroth Landau level and the other Landau levels. This can be achieved by applying an in-plane magnetic field[19–21]. The spin filtering effect discussed here does not require the presence of spin-orbit coupling and its experimental verification is within the current technological capabilities.

Acknowledgments

This work was financially supported by the Swiss National Science Foundation (SNSF) and the NCCR Quantum Science and Technology.

* Email address: tibor.sekera@unibas.ch

[1] K.S. Novoselov, Z. Jiang, Y. Zhang, S.V. Morozov, H.L. Stormer, U. Zeitler, J.C. Maan, G.S. Boebinger, P. Kim, and A.K. Geim, Science **315**, 1379 (2007).
[2] H.B. Heersche, P. Jarillo-Herrero, J.B. Oostinga, L.M.K. Vandersypen, and A.F. Morpurgo, Nature **446**, 56 (2007).
[3] D. Jeong, J.-H. Choi, G.-H. Lee, S. Jo, Y.-J. Doh, and H.-J. Lee, Phys. Rev. B **83**, 094503 (2011).
[4] G.-H. Lee, S. Kim, S.-H. Jhi, and H.-J. Lee, Nat. Commun. **6**, 6181 (2015).
[5] P. Rickhaus, M. Weiss, L. Marot, and C. Schönenberger, Nano Lett. **12**, 1942 (2012).
[6] G.-H. Park, M. Kim, K. Watanabe, T. Taniguchi, and H.-J. Lee, Sci. Rep. **7**, 10953 (2017).
[7] G.-H. Lee, K.-F. Huang, D.K. Efetov, D.S. Wei, S. Hart, T. Taniguchi, K. Watanabe, A. Yacoby, and P. Kim, Nat. Phys. **13**, 693 (2017).
[8] P. San-Jose, J.L. Lado, R. Aguado, F. Guinea, and J. Fernández-Rossier, Phys. Rev. X **5**, 041042 (2015).
[9] F. Finocchiaro, F. Guinea, and P. San-Jose, Phys. Rev. Lett. **120**, 116801 (2018).
[10] N.M.R. Peres, F. Guinea, and A.H. Castro Neto, Phys. Rev. B **73**, 125411 (2006).
[11] L. Brey and H.A. Fertig, Phys. Rev. B **73**, 195408 (2006).
[12] D.A. Abanin, P.A. Lee, and L.S. Levitov, Phys. Rev. Lett. **96**, 176803 (2006).
[13] A.R. Akhmerov and C.W.J. Beenakker, Phys. Rev. Lett. **98**, 157003 (2007).
[14] J. Tworzydło, I. Snyman, A.R. Akhmerov, and C.W.J. Beenakker Phys. Rev. B **76**, 035411 (2007).
[15] A.V. Volkov, A.A. Shylau, and I.V. Zozoulenko, Phys. Rev. B **86**, 155440 (2012).
[16] C.W.J. Beenakker, Phys. Rev. Lett. **97**, 067007 (2006).
[17] D. Greenbaum, S. Das, G. Schwiete, and P. G. Silvestrov, Phys. Rev. B **75**, 195437 (2007).
[18] C.W. Groth, M. Wimmer, A.R. Akhmerov, and X. Waintal, New J. Phys. **16**, 063065 (2014).
[19] A.J.M. Giesbers, L.A. Ponomarenko, K.S. Novoselov, A.K. Geim, M.I. Katsnelson, J.C. Maan, and U. Zeitler, Phys. Rev. B **80**, 201403(R) (2009).
[20] E.V. Kurganova, H.J. van Elferen, A. McCollam, L.A. Ponomarenko, K.S. Novoselov, A. Veligura, B.J. van Wees,

J.C. Maan, and U. Zeitler, Phys. Rev. B **84**, 121407(R) (2011).
[21] F. Chiappini, S. Wiedmann, K. Novoselov, A. Mishchenko, A.K. Geim, J.C. Maan, and U. Zeitler, Phys. Rev. B **92**, 201412(R) (2015).